Approach to Interfacial and Intramolecular Electron Transfer of the Diheme Protein Cytochrome c_4 Assembled on Au(111) Surfaces

Qijin Chi,*,† Jingdong Zhang,† Taner Arslan,† Lotte Borg,† Gert W. Pedersen,† Hans E. M. Christensen,† Renat R. Nazmudtinov,‡ and Jens Ulstrup*,†

Department of Chemistry and Nano•DTU, Technical University of Denmark, Kemitorvet, Building 207, DK-2800 Kongens Lyngby, Denmark, and Kazan State Technological University, 420015 Kazan, Republic of Tatarstan, Russian Federation

Received: January 25, 2010; Revised Manuscript Received: March 13, 2010

Intramolecular electron transfer (ET) between metal centers is a core feature of large protein complexes in photosynthesis, respiration, and redox enzyme catalysis. The number of microscopic redox potentials and ET rate constants is, however, prohibitive for experimental cooperative ET mapping, but two-center proteins are simple enough to offer complete communication networks. At the same time, multicenter redox proteins operate in membrane environments where conformational dynamics may lead to gated ET features different from conditions in homogeneous solution. The bacterial respiratory diheme protein *Pseudomonas stutzeri* cytochrome c_4 has been a target for intramolecular, interheme ET. We report here voltammetric and *in situ* scanning tunneling microscopy (STM) data for *P. stutzeri* cyt c_4 at single-crystal, atomically planar Au(111)-electrode surfaces modified by variable-length ω-mercapto-alkanoic carboxylic acids. As evidenced by *in situ* STM, the strongly dipolar protein is immobilized in a close to vertical orientation at this surface with the positively charged high-potential heme domain adjacent to the electrode. This orientation gives asymmetric voltammograms with two one-ET peaks in the cathodic direction and a single two-ET peak in the anodic direction. Intramolecular, interheme ET with high, 8,000−30,000 s^{-1}, rate constants is notably an essential part of this mechanism. The high rate constants are in striking contrast to ET reactions of *P. stutzeri* cyt c_4 with small reaction partners in homogeneous solution for which kinetic analysis clearly testifies to electrostatic cooperative effects but no intramolecular, interheme ET higher than 0.1−10 s^{-1}. This difference suggests a strong gating feature of the process. On the basis of the three-dimensional structure of *P. stutzeri* cyt c_4, gating is understandable due to the through-space, hydrogen-bonded electronic contact between the heme propionates which is highly sensitive to environmental configurational fluctuations.

1. Introduction

Biological electron transfer (ET) function in photosynthetic reaction centers,[1,2] respiratory complexes such as cytochrome *c* oxidase,[3−5] and redox enzymes[6−10] is controlled by large protein complexes with several transition metal centers. Communication between the membrane bound complexes is by small mobile ET carriers such as cytochrome *c*, plastocyanine, or quinones. The electronic conductivity through the protein complexes is determined by thermodynamic properties, say equilibrium redox potentials, coupling of the redox centers to the protein matrix and aqueous/membrane interfacial environment, and the relative distance and orientation of the ET centers.

Two other issues regarding long-range multi-ET "hopping" in redox (metallo)proteins require attention. The large number of microscopic interactions in multicenter redox proteins[11,12] is, first, prohibitive for complete microscopic thermodynamic and ET reactivity mapping with "cooperativity" included. Prototype *two-center* redox metalloproteins offer, however, complete mapping where the respiratory bacterial diheme protein cytochrome c_4 from *Pseudomonas stutzeri* has been a central target protein.[13−15] Figure 1 shows a three-dimensional structural representation of this protein, along with monoheme cytochrome *c* as a reference. The surface charge distribution and heme centers of *P. stutzeri* cyt c_4 are shown in Figure 2. Thermodynamic,[13−16] folding,[17] spectroscopic,[13,18,19] and ET kinetic properties[13,14,20,21] are also available.

The preparation of the particular nuclear configuration in which ET occurs can, second, be critical. "Gated" ET is a notion used for this phenomenon[26] that implies expenditure of additional activation free energy in return for a more facile electronic transmission coefficient. This feature is important when ET is mediated in part by through-space links and particularly if ET is accompanied by proton transfer (PT), as the latter is spatially much more strongly confined than ET. The electronic transmission coefficient of intramolecular ET via a through-space link could thus assume widely different values in different environments such as bulk solution or in membrane or in interfacial electrochemical environment.

The following observations are important when gated intramolecular ET between the two heme groups in *P. stutzeri* cyt c_4 is addressed:[13]

- The 190-residue protein is organized in two almost equal-size globular domains, each with a heme group and connected by a 12-residue peptide chain.[22,25] The protein is strongly dipolar with excess negative and positive charge (pH 7) of the N- and C-terminal domain, respectively. This property is crucial for the electrostatic immobilization of the protein in

* Corresponding authors. Phone: +45 252032 (Q.C.); +45 252359 (J.U.). Fax: +45 883136 (Q.C.); +45 883136 (J.U.). E-mail: cq@kemi.dtu.dk (Q.C.); ju@kemi.dtu.dk (J.U.).
† Technical University of Denmark.
‡ Kazan State Technological University.

10.1021/jp1007208
Published on Web 04/01/2010

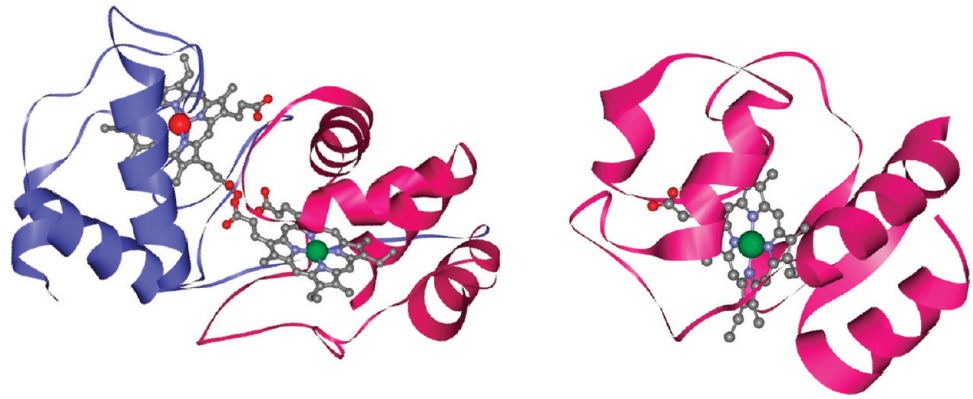

Figure 1. Left: Three-dimensional structure of *P. stutzeri* cyt c_4. The N- and C-terminal domains (in blue and red, respectively), the linking peptide, the heme groups, and the propionate hydrogen bond contact are shown. Right: Similar representation of horse heart cyt *c*. Coordinates from[22] PDB code 1EPT (cyt c_4) and[23] PDB 1HRC (cyt *c*). Graphics in Molscript.[24]

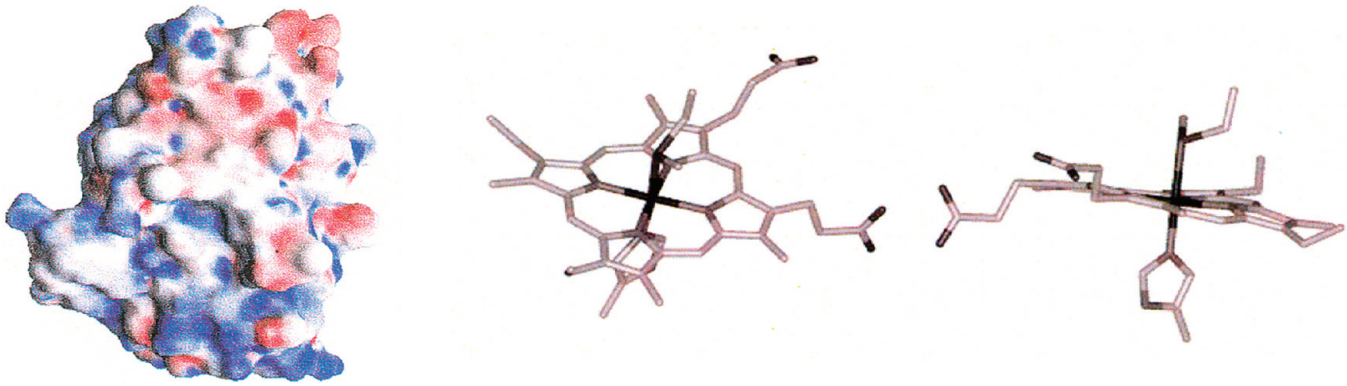

Figure 2. Left: Surface charge distribution of *P. stutzeri* cyt c_4. Red and blue show negative (N-terminal domain) and positive (C-terminal domain) charge distributions, respectively. Data from refs 13 and 25. Right: The heme groups with axial ligands and the propionate hydrogen bond contact.

well-defined specific orientations on electrode surfaces functionalized by self-assembled molecular monolayers (SAMs).

- The heme groups are strongly hydrogen bonded via two heme propionates. The 19 Å Fe−Fe distance implies that electronic contact for efficient interheme ET is established. However, by the propionate-mediated contact length and involvement of a noncovalent, albeit strongly H-bonded link, the cyt c_4 structure also suggests that intramolecular ET between the heme groups is at the boundary between the adiabatic and diabatic limits of strong and weak electronic coupling, respectively,[15,21] and therefore particularly subject to environmental fluctuational gating.
- Electrostatic computations combined with Monte Carlo sampling suggest that PT between the propionates could accompany intraheme ET.[25] As noted, PT involvement would strongly enhance further the sensitivity to configurational gating, cf. section 4.
- Bimolecular ET of *P. stutzeri* cyt c_4 with inorganic reaction partners[14,21] and with flavin and methylviologen radicals[20] in homogeneous solution has been studied extensively. The two- or three-phasic kinetic patterns could map the microscopic reduction potentials. Macroscopic bulk potentials of the N- and C-terminal hemes are about 240 and 330 mV (NHE), respectively, but these values are modified by 30−40 mV electrostatic "cooperative" effects.[14] No evidence of intramolecular ET between the heme groups could, however, be detected in time ranges of 0.1−10 $s^{14,21}$ most likely due to competition by faster *inter*molecular ET with the reaction partners.
- Cyclic voltammetry offers an approach to intraheme ET in *P. stutzeri* cyt c_4 that circumvents intermolecular ET.[16] Diffusion controlled voltammetry on polycrystalline Au-electrodes modified by thiol-based SAMs with positively (ammonium group) or negatively charged functional groups (carboxylate group) suggest that *P. stutzeri* cyt c_4 is oriented on the surface with either the negatively (N-terminal, low-potential heme) or positively charged (C-terminal, high-potential heme) domain facing the surface. Interfacial two-ET is then *only* possible by ET between the electrode surface and the adjacent heme group, followed by interheme ET between the adjacent and remote heme group. This view is central in the present communication. The diffusion controlled voltammograms showed intriguing asymmetry that supports this view.[16] For example, if the high-potential C-terminal heme group is adjacent to the electrode surface, this group is reduced first in a cathodic scan followed by reduction of the remote heme group at the lower potential of the latter. *Two one-electron* peaks are therefore expected. In the reverse scan, the low-potential remote heme group cannot, however, be reoxidized until the potential of the adjacent high-potential heme group is reached. *A single two-electron* peak is therefore expected. A reverse pattern is expected when the low-potential heme group is adjacent to the surface. Details of these patterns offer a route to the intramolecular ET rate constants. Numerical analysis of these data[16] pointed to significant intramolecular ET rate constants, i.e., around 40 s^{-1} for the $C_{terminal} \rightarrow N_{terminal}$ ET process and $\approx 10^3$ s^{-1} for the $N_{terminal} \rightarrow C_{terminal}$ ET process[16] (the two rate constants are related by the

equilibrium redox potential difference of the heme groups). Values in these ranges in homogeneous solution would have been disclosed as fast *intra*molecular electronic equilibrium, but as noted, this was not observed. A likely reason is that intramolecular ET is much slower in homogeneous solution than at the electrochemical interface. Binding to the SAM-modified electrode surface seems to trigger intramolecular ET. This raises issues about the sensitivity of the electronic tunneling factor to environmental gating.

The data reported in ref 16 were fraught with interference from diffusion and by limited voltammetric resolution. In the present report, we address electrochemically controlled intramolecular ET between the two heme groups in *P. stutzeri* cyt c_4 immobilized in well oriented molecular monolayers on single-crystal, atomically planar Au(111)-electrode surfaces modified by variable-length ω-mercapto alkanoic carboxylic acids. Scanning tunneling microscopy directly in the aqueous buffer under potential control (*in situ* STM) supports the expected surface orientation. This quality of electrode surfaces strongly enhances the voltammetric sensitivity and together with *in situ* STM leads to unequivocal conclusions as to both the mechanism of the two-ET cyt c_4 oxidation and reduction and precise (high) values of the intramolecular ET rate constants.

2. Experimental Section

2.1. Materials and Reagents. The ω-mercapto alkanoic carboxylic acids ($HS(CH_2)_nCOOH$, $n = 2, 5, 7, 10, 11, 15, 17$) were obtained from various companies and used as received. 3-Mercaptopropionic acid ($HS(CH_2)_2COOH$, 99%) and 11-mercapto-undecanoic acid ($HS(CH_2)_{10}COOH$, 99%) were obtained from Sigma-Aldrich. 5-Carboxyl-1-pentanethiol ($HS(CH_2)_5COOH$, 98%) and 7-carboxyl-1-heptanethiol ($HS(CH_2)_7COOH$, 98%) were obtained from Dojindo (Japan), and 12-mercaptododecanoic acid ($HS(CH_2)_{11}COOH$, 90%), 16-mercapto-hexadecanoic acid ($HS(CH_2)_{15}COOH$, 90%), and 18-mercapto-tetradecanoic acid ($HS(CH_2)_{17}COOH$, 90%) were obtained from ProChimia (Poland). KH_2PO_4 (99.99%) and K_2HPO_4 (99.99%) were from Aldrich and Fluka, respectively. Ethanol (ultrapure, Merck) was used to prepare thiol solutions. Other reagents used in protein production and purification were at least of analytical grade. Phosphate buffer was prepared by mixing of KH_2PO_4 and K_2HPO_4 solutions. The solution pH was monitored by pH meter (Radiometer Danmark, Denmark). Milli-Q water (18.2 MΩ cm) was used throughout.

Both homemade Au(111) electrodes[27a−c] prepared from polycrystalline gold wire (99.99%) and commercial Au(111) substrates from Surface Preparation Laboratory (The Netherlands) were used. The quality of the homemade Au(111) surfaces was checked in 0.1 M $HClO_4$ and 0.1 M H_2SO_4 by both electrochemistry and *in situ* STM. Both main and detailed (fingerprint) features accorded with literature reports.[27a] No significant difference between homemade and commercial Au(111) surfaces was found through all the experiments.

2.2. Preparation of Cytochrome c_4 and N-Terminal Domain Samples. Recombinant *P. stutzeri* cyt c_4 was expressed using the previously developed expression system.[28] An expression system for N-terminal *P. stutzeri* cyt c_4 was created by introducing a stop codon in the gene after amino acid 90. Cells expressing recombinant *P. stutzeri* cyt c_4 and N-terminal cyt c_4 were prepared in minimal media as previously described.[19] The proteins were then purified as described[28] and stored as stock solutions in 5 mM Tris/HCl, pH 7.5, 100 mM NaCl. Fully oxidized and fully reduced protein samples were prepared by adding a 5-fold excess of 10^{-4} M $K_3[Fe(CN)_6]$ in 5 mM Tris/HCl, pH 7.5, 100 mM NaCl, or 1 mM sodium ascorbate, respectively. After 1 h of incubation, the buffer was changed into 5 mM phosphate buffer by ultrafiltration using a stirred Amicon cell pressurized by nitrogen and fitted with a Diablo YM3 membrane.

2.3. Preparation of cyt c_4 Monolayers. The freshly quenched Au(111) electrodes were immersed in 1 mM ω-mercapto alkanoic carboxylic acid in ethanol overnight, followed by rinsing with ethanol and Milli-Q water. The electrodes were then transferred to cyt c_4 solution (ca. 40 μM in phosphate buffer) for adsorption for 20 h.

2.4. Electrochemical Measurements. Cyclic voltammetry was conducted using an Autolab electrochemical system (Eco Chemie, The Netherlands) controlled by the general-purpose electrochemical system software. The electrochemical setup including cell and three-electrode configuration was cleaned and employed as previously done.[27b−d] Clean Pt wire was used as a counter electrode. The reference electrode was a freshly prepared reversible hydrogen electrode (RHE), checked against a saturated calomel electrode (SCE) after each measurement. All potentials are reported versus SCE. Cyt c_4/SAM/Au(111) was the working electrode. The Au(111)-electrode was prepared by annealing in a hydrogen flame, quenched in dihydrogen saturated Millipore water, and transferred to the SAM-forming solution for adsorption. This was followed by adsorption in 40 μM cyt c_4 solutions for 20 h. Electrolyte solutions were deoxygenated by argon (99.999%) purified further by Chrompack (oxygen <50 ppb) for about 1 h before measurements, and the argon atmosphere kept during measurements.

2.5. STM Imaging. A Pico SPM instrument (Molecular Imaging Co., USA) was used for *in situ* STM measurement. Tungsten tip or Pt/It (80/20) tip was homemade by electrochemical etching and coated with Apiezon wax.[27d] The *in situ* STM scanner was calibrated as described.[27d] All images were recorded under argon as described previously.[30]

3. Results

3.1. Electrostatic Immobilization and In Situ STM of Cyt c_4 on Au(111)-Electrode Surfaces Modified by ω-Mercapto Alkanoic Acid SAMs. With a positively and a negatively charged domain, *P. stutzeri* cyt c_4 can be immobilized by electrostatic forces on functionalized SAMs with complementary charges, illustrated schematically in Figure 3. The domain charges match the equilibrium redox potentials; i.e., the high-potential heme is accommodated in the positively charged C-terminal and the low-potential heme group in the negatively charged N-terminal domain. This leads to unidirectional electron flow through the protein controlled by intramolecular ET between the two heme groups.

Figure 4 shows *in situ* STM images of submonolayers of cyt c_4 (b) and cyt c (c) on a ω-mercapto-undecanoic acid SAM-covered Au(111)-electrode surface in 5 mM phosphate buffer (pH 7.0). The STM image of ω-mercapto-undecanoic acid SAM alone (i.e., no protein) is included as a reference, Figure 4a. Both proteins display high-quality monolayer voltammetry on these surfaces, section 3.2. The sharp roughly circular contrasts are close to the crystallographic size of cyt c or a single cyt c_4 domain, strongly suggesting that the contrasts represent individual cyt c_4 or cyt c molecules with cyt c_4 in an upright, i.e., vertical orientation. This is supported by comparison with the N-terminal cyt c_4 domain alone, for which no stable adsorption on the thiol-modified Au(111) surfaces could be detected (data not shown).

3.2. Cyclic Voltammetry of Oriented Cyt c_4 on SAM-Modified Au(111)-Electrode Surfaces. Figure 5 shows cyclic voltammograms (CVs) of *P. stutzeri* cyt c_4 and of cyt c, both on ω-mercapto-decanoic acid SAM-modified Au(111)-electrode

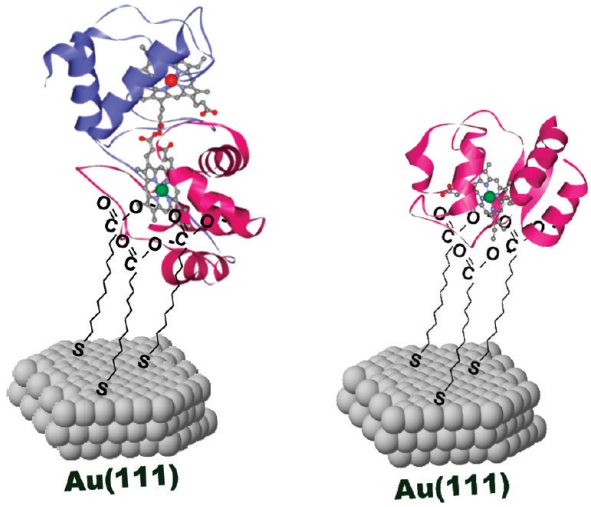

Figure 3. Illustration of the most favorable molecular orientation of *P stutzeri* cyt c_4 on electrostatic immobilization via the positively (C-terminal, marked red, high-potential heme adjacent to the electrode surface, left). Immobilization of single-heme horse heart cyt *c* shown to the right.

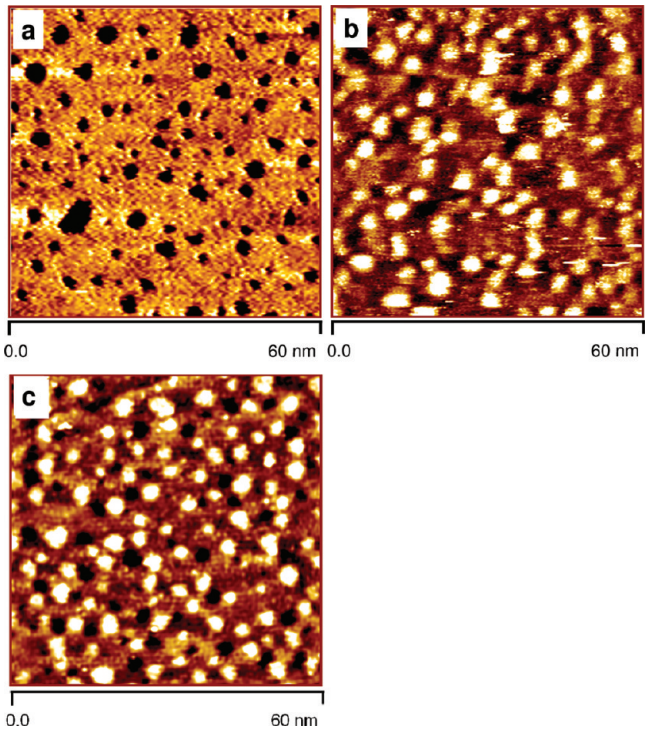

Figure 4. *In situ* STM images of (a) a ω-mercapto-decanoic acid SAM-modified Au(111)-electrode surface without protein, (b) with *P. stutzeri* cyt c_4, and (c) with horse heart cyt *c* monolayers. The images were acquired in constant current mode in phosphate buffer (5 mM, pH 7.0) under electrochemical potential control. Scan area, 60 × 60 nm^2; working electrode potential, 0.15 V (vs SCE); bias voltage, −0.43 V; tunneling current, 0.15 nA.

surfaces. The latter CV (Figure 5b) follows previously observed voltammetric behavior of cyt *c* on polycrystalline electrodes modified by carboxylate-functionalized alkanethiols.[31−33] Notably, the CV of *P. stutzeri* cyt c_4 shows an entirely different pattern. The cathodic scan shows two distinct peaks at about −230 and −370 mV (SCE), while the anodic scan shows a single, approximately twice as large peak at about −75 mV (SCE).

This behavior follows the pattern for an oriented cyt c_4 (sub)-monolayer with the positively charged, high-potential heme

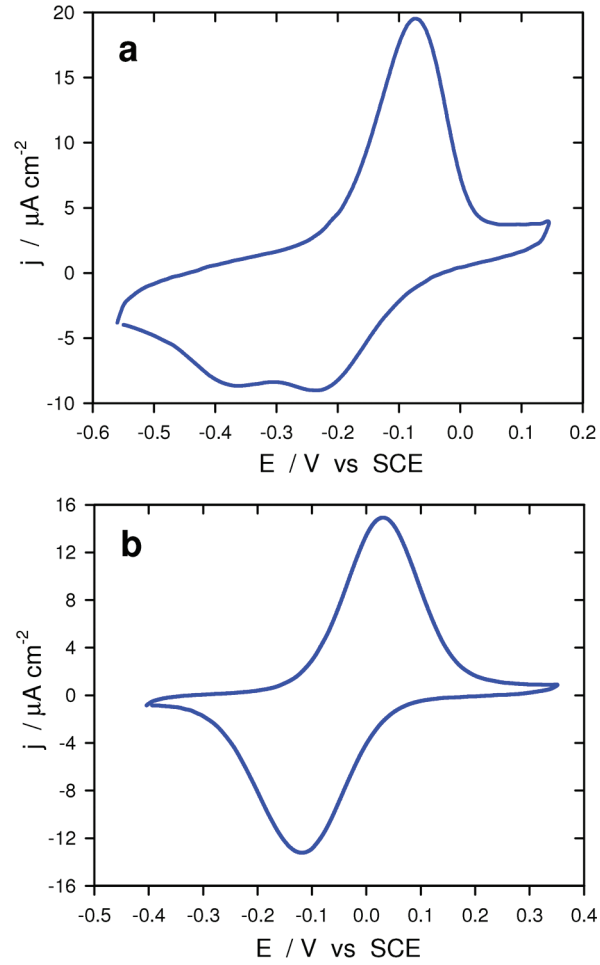

Figure 5. Representative cyclic voltammograms of *P. stutzeri* cyt c_4 (a) and horse heart cyt *c* (b) monolayers on ω-mercapto-decanoic acid SAM-covered Au(111)-electrode surfaces in phosphate buffer (5 mM, pH 7.0). Scan rate: 2 V s^{-1}. The cyt c_4 orientation corresponds to the orientation shown in Figure 3a.

adjacent to the electrode. The voltammograms are much better resolved than for diffusion controlled voltammograms of *P. stutzeri* cyt c_4 on modified polycrystalline electrode surfaces.[16] This is due to the absence of diffusion effects and the much better defined single-crystal Au(111)-electrode environment. The peak potentials are significantly lower, i.e., by 200−300 mV, than determined by forward and reverse ET rate constants in bulk solution[14] or by diffusion controlled voltammetry at differently modified polycrystalline electrode surfaces.[16] Such differences have also been observed for the Fe_3S_4 iron−sulfur protein *Pyrococcus furiosus* ferredoxin[34] and can be at least partially ascribed to the strongly negatively charged interfacial electrochemical environment at the carboxylate-modified Au(111)-electrode surfaces.

The rationale for asymmetric voltammograms such as in Figure 5 is that on cathodic scanning the adjacent high-potential heme is reduced first, followed by reduction of the remote, low-potential heme via intramolecular ET from the adjacent to the remote heme. Thermodynamically, the low-potential, remote heme group would be reoxidized first in the reverse, anodic scan, but this cannot be achieved until the potential of the adjacent high-potential heme is reached. Fast two-ET then follows. The overall voltammetric shape depends also on the scan rate, as shown in Figure 6, and both the interfacial electrochemical ET and the intramolecular ET kinetics. This

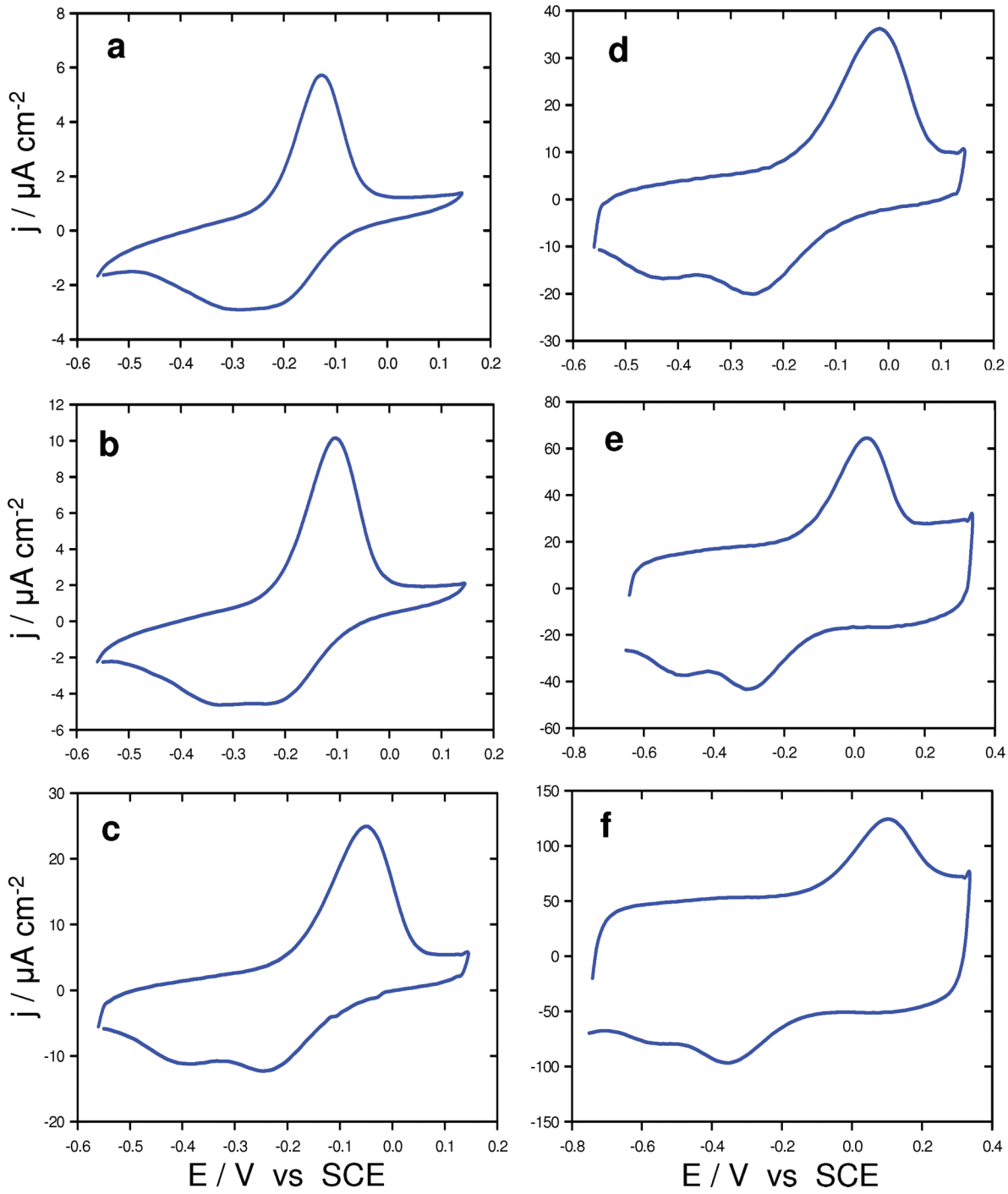

Figure 6. Cyclic voltammograms of *P. stutzeri* cyt c_4 (sub)monolayers on ω-mercapto-decanoic acid SAM-covered Au(111)-electrode surfaces in phosphate buffer (5 mM, pH 7.0) obtained with various scan rates: (a) 0.5, (b) 1.0, (c) 3.0, (d) 5.0, (e) 10, and (f) 20 V s^{-1}.

allows us to estimate the rate constants of both the interfacial and the intramolecular ET.

3.3. Rate Constants of Interfacial Electrochemical and Intramolecular ET of Immobilized Cyt c_4. The combined interfacial electrochemical and intramolecular ET processes are represented by the scheme shown in Figure 7a. The two-ET voltammograms have been simulated numerically using an in-house program written in MathCad, described elsewhere[8,35] and previously applied to gold nanoparticle-mediated interfacial electrochemical ET of cyt c[36] and to the electrocatalysis of the two-center redox metalloenzyme, copper nitrite reductase.[8]

The detailed voltammetric shape is particularly sensitive to the ratio between the interfacial standard electrochemical, k_1, and the intramolecular, interheme ET rate constant, k_2. For example, a large k_1/k_2 ratio ($\cong$10) and fast intramolecular ET compared to the scan rate gives a single set of two-ET peaks. Small scan rates and k_1/k_2 ratios less than about 10 give two successive peaks in both cathodic and anodic scans, while large scan rates compared to the intramolecular ET rate only give a single pair of single-ET peaks as intramolecular ET here cannot follow along with the potential scans. The best accordance with the data is obtained when the scan rate (time) is comparable with the intramolecular ET rate (time) and the latter rate constant, k_2, significantly exceeds the standard interfacial electrochemical ET rate constant, k_1. A simulated voltammogram (with no background) that accords closely with the data (not

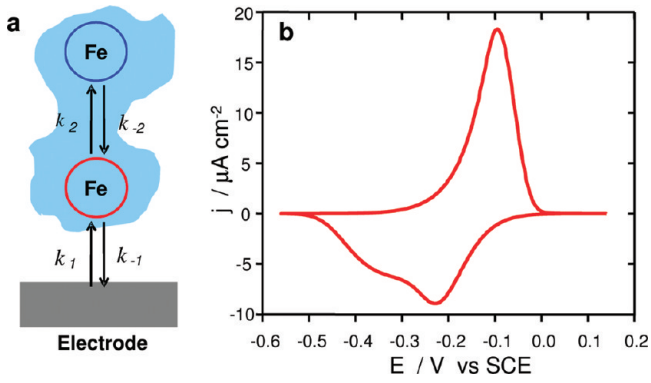

Figure 7. Schematic view of *P stutzeri* cyt c_4 interfacial electrochemical ET including intramolecular, interheme ET (a) and a simulated voltammogram for cyt c_4 on 11-mercapto-undecanoic acid modified Au(111) surface (b). Parameters used in the simulation: $k_1 = 15\ s^{-1}$, $k_2 = 18\ 000\ s^{-1}$, and scan rate 2 V s^{-1}.

TABLE 1: Rate Constants of Interfacial ET and Intramolecular ET Obtained by Electrochemical Measurements and Simulated Voltammograms

distance (number of CH_2 groups)	interfacial ET rate constants (k_{IF}, s^{-1})	intramolecular ET rate constants (k_{IM}, s^{-1})
2	740 ± 100	30000 ± 3000
5	700 ± 100	25000 ± 3000
7	200 ± 100	20000 ± 3000
10	15 ± 4	18000 ± 3000
11	5 ± 2	15000 ± 2000
15	0.6 ± 0.1	10000 ± 2000
17	0.09 ± 0.02	8000 ± 2000

corrected for background currents) is shown in Figure 7b. Substantiation of this pattern is provided by CVs of *P. stutzeri* cyt c_4 on Au(111)-electrode surfaces modified by variable-length ω-mercapto-alkanoic acid SAMs. The rate constants extracted from these data are collected in Table 1 and shown in Figure 8. The following is noted:

- The voltammetric shapes and kinetic data follow closely the two-ET views represented by Figures 5 and 7.
- The interfacial electrochemical ET rate constants follow a consistent bimodal pattern previously observed for horse heart cyt *c*[31−33] and *Pseudomonas aeruginosa* azurin.[37] The bimodal pattern has been assigned to an overall two-step process with a preorganization step followed by the interfacial ET step itself. The former is rate determining for short chain lengths, the latter for longer lengths. The distance dependence of the rate constant for SAM molecular lengths larger than ≅6 methylene groups is exponential. Assuming a value of 30° for the angle between the alkanethiol chain and the surface normal an exponential fitting to the distance dependent rate constant: $k_{IF}(x) = k^0_{IF} \exp(-\beta x)$ gave a β value of ca. 0.8 $Å^{-1}$, which agrees broadly with similar estimates reported for other redox couples attached to a gold electrode through alkanethiol monolayers.[38,39]
- The intramolecular ET rate constant emerges consistently with large values, i.e., $(8-30) \times 10^3\ s^{-1}$. There is also here a systematic dependence on the SAM thickness, but the apparent decay factor, ≅ 0.09 per methylene group, is very low and in no way reflects systematic tunneling behavior. This weak variation instead reflects small systematic, elusive but perfectly conceivable environmental variation as the interfacial composition is gradually changed. Similar systematic weak variation of the reductive desorption potential of variable-length alkane thiols with hydrophobically bound azurin on top has also been observed.[37] The intramolecular ET rate constants obtained can therefore be regarded as virtually constant throughout the series of ω-mercapto-undecanoic acid SAMs.

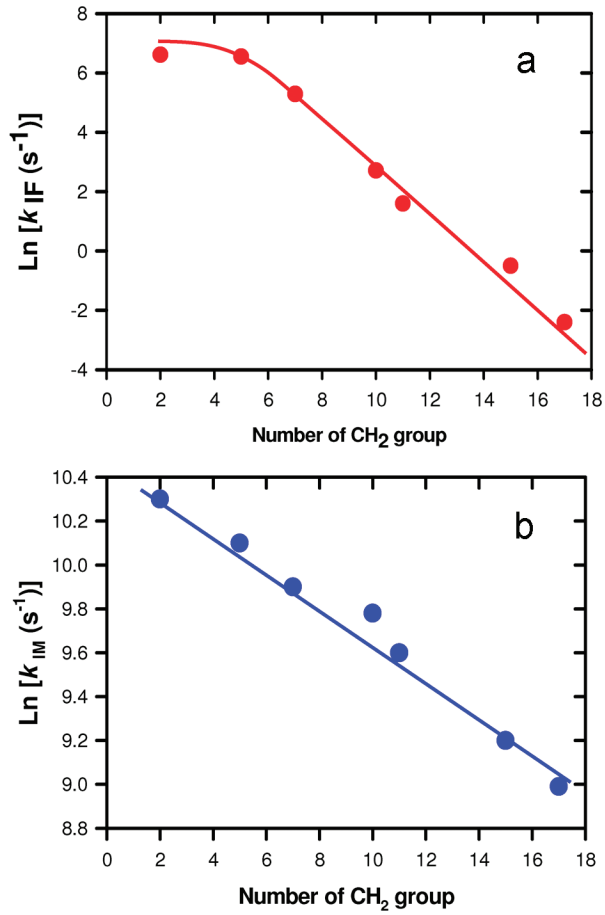

Figure 8. Dependence of rate constants on the interfacial ET distance (denoted by the number of $-CH_2$ groups) in the ω-mercapto-alkanoic acid SAM modified Au(111)-electrode surface: (a) the interfacial electrochemical ET step; (b) the intramolecular, interheme ET step.

4. Discussion

The strongly dipolar, diheme redox metalloprotein *P. stutzeri* cyt c_4 can be immobilized in controlled orientations on Au-electrodes modified by negatively or positively charged SAMs. This was also exploited in a recent study of wild-type and mutant *Pseudoalteromonas haloplanktis* cyt c_4 in either free or immobilized state.[40] We have specifically addressed *P. stutzeri* cyt c_4 submonolayers on Au(111)-electrode surfaces modified by variable-length negatively charged ω-mercapto-decanoic acid SAMs. CVs on these well-defined, atomically planar surfaces show all the features of unidirectional electron flow through the protein with intramolecular ET between the two heme groups as a decisive controlling feature. The oriented adsorption with cyt c_4 in an upright orientation is strongly supported by *in situ* STM of both cyt c_4 and single-heme cyt *c* to single-molecule resolution, as well as by the complete absence of negatively charged *P stutzeri* N-terminal cyt c_4 adsorption. The high voltammetric resolution compared with previous studies of cyt c_4 voltammetry based on diffusion control and polycrystalline Au-electrode surfaces has enabled determining the interfacial electrochemical ET rate constant and the intramolecular, interheme ET rate constants with high precision.

The kinetic data substantiate that the intramolecular, interheme ET process of surface immobilized *P. stutzeri* cyt c_4 is indeed fast. Rate constants in the microsecond range,

$k_2 \cong 10^4\ s^{-1}$ for the C → N terminal interheme ET process emerge from the kinetic analysis. These values are an order of magnitude higher than previously estimated from diffusion controlled *P. stutzeri* cyt c_4 voltammetry at polycrystalline Au-electrode surfaces.[16] In view of the hypersensitivity of the electronic transmission coefficient to nuclear gating, this difference is hardly surprising. The huge difference between virtual absence of intramolecular ET in *P. stutzeri* cyt c_4 in homogeneous solution[14,21] and fast intramolecular ET in immobilized *P. stutzeri* cyt c_4 is much more notable. Moreover, while the rate constants of interfacial electrochemical ET follow expected tunneling distance decay, the intramolecular ET rate constant is close to constant, substantiating the nature of the latter process as a true intramolecular process.

The huge difference between the very low intramolecular ET rate constants of *P. stutzeri* cyt c_4 in homogeneous solution and immobilized at well-defined electrochemical electrode surfaces strongly point to environmental configuration gating of the intramolecular, interheme ET process. The three-dimensional crystal structure of *P. stutzeri* cyt c_4 offers a clue to this view. The noncovalent H-bond contact, possibly involving accompanying proton transfer, is thus exceedingly sensitive to the propionate contact distance. Even tiny fluctutation effects constitute a highly efficient on−off ET mechanism. This could reflect the occurrence of *P. stutzeri* cyt c_4 both in the periplasmic cellular space and in the membrane bound state.[13]

The importance of gating can be illuminated by the preliminary theoretical frame below. The determining ET factors are reflected in the following equations for the rate constant of the fundamental intramolecular ET process[41,42]

$$W_{RP} = \kappa_{el}\frac{\omega_{eff}}{2\pi}\exp\left[-\frac{(E_r + \Delta G^0)^2}{4E_r k_B T}\right] \quad (1)$$

$$\kappa_{el} = (T_{RP})^2\sqrt{\frac{4\pi^3}{E_r k_B T \hbar^2 \omega_{eff}{}^2}} \text{ if } \kappa_{el} \ll 1, \text{ otherwise } \kappa_{el} \to 1 \quad (2)$$

ΔG^0 in eq 1 is the reaction free energy, E_r the total solvent, protein, membrane, and intramolecular reorganization free energy, ω_{eff} the effective vibrational frequency of all of the nuclear modes reorganized, k_B Boltzmann's constant, T the temperature, and $\hbar$ Planck's constant divided by 2π. T_{RP} in the transmission coefficient, eq 2, is the electronic coupling (tunneling factor) between the reactants' and products' states through the protein medium, at the crossing of the reactants' and products' potential free energy surfaces. A common simple form in the diabatic limit of weak electronic coupling is[42]

$$\kappa_{el} \approx \kappa_{el}^0\left(\frac{\beta}{\Delta}\right)^{2M} \to \kappa_{el}^0\exp\left[-\frac{2}{a}\ln\left(\frac{\Delta}{\beta}\right)R\right] \quad (3)$$

where κ_{el}^0 is a constant, β the average near-neighbor electronic coupling, and Δ the average energy gap of each intermediate state, say atom[43] or amino acid residues[44] counted from the electronic donor group energy. M is the number of intermediate groups, a the average structural extension of the each group, and R the donor−acceptor distance along a particular ET route ($R \cong aM$). Involvement of proton transfer via the propionate link would modify eq 3 to the form

$$\kappa_{el} \approx \kappa_{el}^0\left(\frac{\beta}{\Delta}\right)^{2M}\left(\frac{\beta_H}{\Delta_H}\right)^2; \quad \left(\frac{\beta_H}{\Delta_H}\right)^2 \approx \exp\left[-\frac{m_H\Omega_H(\Delta R_H)^2}{2\hbar}\right] \quad (4)$$

where β_H is the electronic coupling and Δ_H the energy gap for the H-bond contact, m_H and Ω_H the proton mass and vibrational frequency, respectively, and ΔR_H the PT distance *at the fluctuational gated configuration*. Other analysis of gated PT such as this one is available elsewhere.[26,41,42]

The following extension incorporates the gating feature

$$W_{RP} \approx \kappa_{el}^{gated}\frac{\omega_{eff}}{2\pi}\exp\left\{-\frac{w_R(Q^*_{gating}) - w_R(Q^0_{gating})}{k_B T} - \left[\frac{[E_r^{Q^*} + \Delta G^{0Q^*}]^2}{4E_r^{Q^*}k_B T}\right]\right\} \quad (5)$$

$$\kappa_{el}^{gated} = \kappa_{el}S; \quad S \approx \frac{\kappa_{el}(Q_{gating} = Q^*_{gating})}{\kappa_{el}(Q_{gating} = Q^0_{gating})} \gg 1 \quad (6)$$

$w_R(Q^*_{gating}) - w_R(Q^0_{gating})$ is the reversible work to take the donor and acceptor fragments (the heme groups and the propionate contacts) along the gating mode, Q_{gating}, from the equilibrium value of this coordinate, Q^0_{gating}, to the value where ET (and PT) occurs, Q^*_{gating}. κ_{el}^{gating} is similarly the value of the electronic transmission coefficient at $Q_{gating} = Q^*_{gating}$.

By eqs 1−6, the dominating gating effects are in the electronic transmission coefficient, and perhaps the PT term β_H/Δ_H. Gating in the activation free energy terms, $E_r^{Q^*}$ and ΔG^{0Q^*}, is only significant if drastic effects such as electronic spin changes accompany the immobilization process. The gating issue is presently being addressed by density functional computations, but even the simple formalism in eqs 1−6 offers support for the importance of gating in the intramolecular, interheme *P. stutzeri* cyt c_4 ET process. Invoking "suitable" values of the electronic coupling elements in eq 3, based on either atomic[43] or group orbitals,[44] suggests that the intramolecular ET process is a borderline case between the adiabatic and diabatic limits of intramolecular ET.[15,21] This observation substantiates the crucial dependence of the electronic/protonic transmission coefficient to environmental configurational fluctional, or "gating" effects.

The cyt c_4's represented by the *P. stutzeri* cyt c_4 case have offered novel prospects for the understanding of the microscopic cooperation of multicenter photosynthetic, respiratory, and enzyme metalloproteins. Two-center redox metalloproteins also offer other pure and applied[40] perspectives. ET and PT "gating" is one other issue of importance offered by the unique two-center redox metalloproteins. A third perspective offered is the robust nature of this protein in electrochemical interfacial environments and the close (≅100 mV) separation of the redox potentials of the two heme groups. This feature would suggest perspectives based on tunneling spectroscopy for molecular scale electronic device function with conspicuous rectifying (diode-like) properties of the molecule(s) inserted in the *in situ* STM or similar condensed matter molecular scale environments.[45,46]

We have recently explored the electronic coupling using large-scale density functional calculations to address the geometry and electronic structure of the diheme core of cyt c_4 in detail. An original method has been developed to compute the electronic matrix elements (resonance integrals) for large redox pairs. The electronic transmission coefficient of the intramolecular ET was calculated in the framework of Landau−Zener theory for different mutual orientations of the heme groups and Fe−Fe distances. The metal electrode−heme core electronic coupling was also addressed for comparison using the approach developed earlier.[47] The electrostatic contribution to the work terms, and the inner- and outer-sphere reorganization energies, were estimated as well. Deprotonation of the propionate carboxyl group of the heme center was found to play an important role leading to a significant increase in the intramolecular ET rate.

Acknowledgment. Financial support from the Danish Research Council for Technology and Production Sciences (Contract No. 274-07-0272) is acknowledged.

References and Notes

(1) Michel-Beyerle, M. E., Small, G. J., Eds. *Chem. Phys.* **1995**, *197*, 223−472 (special issue on Photosynthesis and the Bacterial reaction Center).

(2) Chuang, J. I.; Boxer, S. G.; Holten, D.; Kirmaier, C. *Biochemistry* **2006**, *45*, 3845–3851 (and references therein).

(3) Tsukihara, T.; Aoyama, H.; Yamashita, E.; Tomizaki, T.; Tamaguchi, H.; Shinzawa-Itoh, K.; Nakashima, R.; Taono, R.; Yoshikawa, S. *Science* **1995**, *269*, 1069–1071.

(4) Yoshikawa, S.; Shinzawa-Itoh, K.; Yamashita, E.; Tsukihara, T. In *Handbook of Metalloproteins*; Messerschmidt, A., Huber, R., Poulos, T., Wieghardt, K., Eds.; Wiley: Chichester, U.K., 2001; Vol. 1, pp 348−362.

(5) (a) Belevich, I.; Verkhovskij, M. I.; Wikstrom, M. *Nature* **2006**, *440*, 829–832. (b) Kim, Y. C.; Wikstrom, M.; Hummer, G. *Proc. Natl. Acad. Sci. U.S.A.* **2007**, *104*, 2169–2174.

(6) Schmid, B.; Chiu, H.-J.; Ramakrishnan, V.; Howard, J. B.; Rees, D. C. In *Handbook of Metalloproteins*; Messerschmidt, A., Huber, R., Poulos, T., Wieghardt, K., Eds.; Wiley: Chichester, U.K., 2001; Vol. 2, pp 1025−1036.

(7) Adman, E. T.; Murphy, M. E. P. In *Handbook of Metalloproteins*; Messerschmidt, A., Huber, R., Poulos, T., Wieghardt, K., Eds.; Wiley: Chichester, U.K., 2001; Vol. 2, pp1381−1390.

(8) Welinder, A. C.; Zhang, J.; Hansen, A. G.; Moth-Poulsen, K.; Christensen, H. E. M.; Kuznetsov, A. M.; Bjørnholm, T.; Ulstrup, J. *Z. Phys. Chem.* **2007**, *221*, 1343–1378.

(9) (a) Angove, H. C.; Cole, J. A.; Richardson, D. J.; Butt, J. N. *J. Biol. Chem.* **2002**, *277*, 23374–23381. (b) Burlat, B.; Gwyer, J. D.; Poock, S.; Clarke, T.; Cole, J. A.; Hemmings, A. M.; Cheesman, M. R.; Butt, J. N.; Richardson, D. J. *Biochem. Soc. Trans.* **2005**, *33*, 137–140.

(10) Gwyer, J. D.; Zhang, J.; Butt, J. N.; Ulstrup, J. *Biophys. J.* **2006**, *91*, 3897–3906.

(11) (a) Coutinho, I.; Xavier, A. V. *Methods Enzymol.* **1994**, *243*, 19–140. (b) Paquete, C. M.; Turner, D. L.; Louro, R. O.; Xavier, A. V.; Caterino, T. *Biochim. Biophys. Acta* **2007**, *1767*, 1169–1179.

(12) Paoli, M.; Nagai, K. In *Handbook of Metalloproteins*; Messerschmidt, A., Huber, R., Poulos, T., Wieghardt, K., Eds.; Wiley: Chichester, U.K., 2001; Vol. 1, pp 16−30.

(13) Andersen, N. H.; Christensen, H. E. M.; Iversen, G.; Nørgaard, A.; Scharnagle, C.; Thuesen, M. H.; Ulstrup, J. In *Handbook of Metalloproteins*; Messerschmidt, A., Huber, R., Poulos, T., Wieghardt, K., Eds.; Wiley: Chichester, U.K., 2001; Vol. 1, pp 100−109.

(14) Karlsson, J.-J.; Conrad, L. S.; Ulstrup, J. *Eur. J. Biochem.* **1995**, *231*, 133–141.

(15) Chi, Q.; Zhang, J.; Jensen, P. S.; Nazmudtinov, R. R.; Ulstrup, J. *J. Phys.: Condens. Matter* **2008**, *20*, 374124.

(16) Karlsson, J.-J.; Nielsen, M. F.; Thuesen, M. H.; Ulstrup, J. *J. Phys. Chem. B* **1997**, *101*, 2430–2436.

(17) Andersen, N. H.; Nørgaard, A.; Jensen, T. J.; Ulstrup, J. *J. Inorg. Biochem.* **2002**, *88*, 316–327.

(18) Nissum, M.; Karlsson, J.-J.; Ulstrup, J.; Jensen, P. W.; Smulevich, G. *J. Biol. Inorg. Chem.* **1997**, *2*, 302–307.

(19) Jørgensen, A. M.; Parak, F.; Christensen, H. E. M. *Phys. Chem. Chem. Phys.* **2005**, *7*, 3472–3477.

(20) Andersen, N. H.; Hervás, M.; Navarro, J. A.; De la Rosa, M. A.; Ulstrup, J. *Inorg. Chim. Acta* **1998**, *272*, 109–114.

(21) Raffalt, A.; Schmidt, L.; Christensen, H. E. M.; Chi, Q.; Ulstrup, J. *J. Inorg. Biochem.* **2009**, *103*, 717–722.

(22) Kadziola, A.; Larsen, S. *Structure* **1997**, *5*, 203–216.

(23) Bushnell, G. W.; Louie, G. V.; Brayer, G. D. *J. Mol. Biol.* **1990**, *214*, 585–595.

(24) Kraulis, P. *J. Appl. Crystallogr.* **1990**, *24*, 946–950.

(25) Iversen, G. Molecular Electrostatics and Electron Tunnelling in Metalloproteins. Ph.D. Thesis, Technical University of Denmark, Lyngby, 1996.

(26) Haiss, W.; Albrecht, T.; van Zalinge, H.; Higgins, S. J.; Bethell, D.; Höbenreich, H.; Schiffrin, D. J.; Nichols, R. J.; Kuznetsov, A. M.; Zhang, J.; Chi, Q.; Ulstrup, J. *J. Phys. Chem. B* **2007**, *111*, 6703–6712.

(27) (a) Hamelin, A. *J. Electroanal. Chem.* **1996**, *407*, 1–11. (b) Zhang, J.; Chi, Q.; Nielsen, J. U.; Friis, E. P.; Andersen, J. E. T.; Ulstrup, J. *Langmuir* **2000**, *16*, 7229. (c) Chi, Q.; Zhang, J.; Friis, E. P.; Andersen, J. E. T.; Ulstrup, J. *Electrochem. Commun.* **1999**, *1*, 91–96. (d) Zhang, J.; Bilic, A.; Reimers, J. R.; Hush, N. S.; Ulstrup, J. *J. Phys. Chem. B* **2005**, *109*, 15355–15367.

(28) Thuesen, M. H.; Nørgaard, A.; Hansen, A. M.; Caspersen, M. B.; Christensen, H. E. M. *Protein Expression Purif.* **2003**, *27*, 175–181.

(29) Arslan, T. Studies of Cytochrome c_4 and Variants. M.Sc. Diss., DTU Chemistry, 2005 (in Danish).

(30) Zhang, J.; Ulstrup, J. *J. Electroanal. Chem.* **2007**, *599*, 213–220.

(31) (a) Avila, A.; Gregory, B. W.; Niki, K.; Cotton, T. W. *J. Phys. Chem. B* **2000**, *104*, 2759–2766. (b) Wei, J. J.; Liu, H.; Niki, K.; Waldeck, D. H. *J. Phys. Chem. B* **2004**, *108*, 16912–16917.

(32) (a) Murgida, D. H.; Hildebrandt, P. *J. Phys. Chem. B* **2001**, *105*, 1578–1586. (b) Murgida, D. H.; Hildebrandt, P. *J. Phys. Chem. B* **2002**, *106*, 12814–12819. (c) Murgida, D. H.; Hildebrandt, P. *Acc. Chem. Res.* **2004**, *37*, 854–861.

(33) Yue, H.; Khoshtariya, D.; Waldeck, D. H.; Grochol, J.; Hildebrandt, P.; Murgida, D. H. *J. Phys. Chem. B* **2006**, *110*, 19906–19913.

(34) Zhang, J.; Christensen, H. E. M.; Ooi, B. L.; Ulstrup, J. *Langmuir* **2004**, *20*, 10200–10207.

(35) Welinder, A. C. MathCad Programme for Two-centre Monolayer Voltammetry and Electrocatalysis, DTU Chemistry, Lyngby, 2006. Available on request.

(36) Jensen, P. S.; Chi, Q.; Grumsen, F. B.; Abad, J. M.; Horsewell, A.; Schiffrin, D. J.; Ulstrup, J. *J. Phys. Chem. C* **2007**, *111*, 6124–6132.

(37) (a) Chi, Q.; Zhang, J.; Andersen, J. E. T.; Ulstrup, J. *J. Phys. Chem. B* **2001**, *105*, 4669–4679. (b) Chi, Q.; Farver, O.; Ulstrup, J. *Proc. Natl. Acad. Sci. U.S.A.* **2005**, *102*, 16203–16208. (c) Chi, Q.; Zhang, J.; Jensen, P. S.; Christensen, H. E. M.; Ulstrup, J. *Faraday Discuss.* **2006**, *131*, 181–195.

(38) Smalley, J. F.; Finklea, H. O.; Chidsey, C. E. D.; Linford, M. R.; Creager, S. E.; Ferraris, J. P.; Chalfant, K; Zawodzinsk, T.; Feldberg, S. W.; Newton, M. D. *J. Am. Chem. Soc.* **2003**, *125*, 2004–2013.

(39) Newton, M. D.; Smalley, J. F. *Phys. Chem. Chem. Phys.* **2007**, *9*, 555–572.

(40) Monari, S.; Battistuzzi, G.; Borsari, M.; Di Rocco, G.; Martini, L.; Ranieri, A.; Sola, M. *J. Phys. Chem. B* **2009**, *113*, 13645–13653.

(41) Kuznetsov, A. M. *Charge Transfer in Physics, Chemistry and Biology*; Gordon & Breach: Reading, U.K., 1995.

(42) Kuznetsov, A. M.; Ulstrup, J. *Electron Transfer in Chemistry and Biology. An Introduction to the Theory*; Wiley: Chichester, U.K., 1998.

(43) Beratan, D. N.; Betts, J. N.; Onuchic, J. N. *Science* **1991**, *252*, 1285–1288.

(44) Christensen, H. E. M.; Conrad, L. S.; Mikkelsen, K. V.; Nielsen, M. K.; Ulstrup, J. *Inorg. Chem.* **1990**, *29*, 2808–2816.

(45) Kuznetsov, A. M.; Ulstrup, J. *J. Chem. Phys.* **2002**, *116*, 2149–2165.

(46) Zhang, J.; Kuznetsov, A. M.; Medvedev, I. G.; Chi, Q.; Albrecht, T.; Jensen, P. S.; Ulstrup, J. *Chem. Rev.* **2008**, *108*, 2737–2791.

(47) Nazmutdinov, R. R; Roznyatovskaya, N. V.; Glukhov, D. V.; Manyurov, I.R.; Mazin, V. M.; Tsirlina, G. A.; Probst, M. *Inorg. Chem.* **2008**, *47*, 6659–6673.

JP1007208